ELSEVIER

Journal of Nuclear Materials 252 (1998) 55–62

journal of nuclear materials

Deuterium retention in carbides and doped graphites

M. Mayer *, M. Balden, R. Behrisch

Max-Planck-Institut für Plasmaphysik, EURATOM Association, Boltzmannstr. 2, D-85748 Garching, Germany

Received 14 July 1997; accepted 3 October 1997

Abstract

The retention of 1 keV and 8 keV deuterium implanted in B, Si, and Ti doped graphites and in the carbides B_4C, SiC and TiC up to 6.7×10^{19} D atoms/cm^2 has been studied at room temperature with thermal desorption spectroscopy (TDS) and ion beam analysis. Compared to pyrolytic graphite all doped graphites showed a tendency to increased retention of deuterium, especially the materials with high porosity. For the carbides the saturation concentration in the implantation zone in B_4C is about 0.4 D per target atom and therefore comparable to the saturation concentration of D in graphite. SiC exhibits a significant higher saturation concentration of 0.6 D per target atom, whereas TiC shows a significant lower saturation concentration of 0.15 D per target atom. © 1998 Elsevier Science B.V.

1. Introduction

Fine grain graphites are widely used as first wall materials in today's thermonuclear fusion experiments because of the low nuclear charge, high sublimation temperature and good thermal conductivity. Graphite is also anticipated to be used as first wall material in future thermonuclear fusion experiments such as ITER [1]. Major disadvantages of graphite are, however, its high chemical erosion yield due to the formation of hydrocarbons and the ability of carbon to trap large amounts of hydrogen [2–11]. This may result in large tritium inventories trapped in the vessel walls of future experiments when tritium–deuterium mixtures will be used as fusion fuel [12,13].

The hydrogen inventory trapped in the vessel walls of a thermonuclear fusion experiment is determined by three different processes.

(i) Implantation of energetic hydrogen ions or neutrals until saturation in a shallow surface layer within the implantation range. Saturation of hydrogen in carbon is reached at a high level with a ratio of about 0.4 H/C at room temperature [2,5–10]. The implantation range is, however, only several 10 nm, resulting in a total trapped inventory of the order of several 10^{17} hydrogen atoms/cm^2.

(ii) Migration of hydrogen from the implantation zone into the bulk of the material along grain boundaries or internal porosity of polycrystalline graphites and trapping beyond the implantation zone at damage sites [10,14,15]. The concentration of hydrogen trapped beyond the implantation zone is not well known, but is estimated to be of the order of 10^{-4}–10^{-3}. The migration range is also unknown but may exceed several tons of μm. The inventory trapped by migration into the bulk slowly increases with incident fluence, and saturation is not observed until the highest fluences (4×10^{20} atoms/cm^2) used in the laboratory experiments. At this fluence the inventory trapped beyond the implantation zone is of the order of several 10^{17} hydrogen atoms/cm^2. For incident fluences greater than 10^{21} atoms/cm^2 the hydrogen migrated and trapped beyond the implantation zone exceeds the inventory trapped in the implantation zone. This was also observed in the graphite divertor tiles of the tokamak experiment ASDEX upgrade [16].

(iii) Buildup of codeposited hydrogen–carbon layers by simultaneous bombardment with hydrogen and carbon [11]. The hydrogen concentration in codeposited layers is about

* Corresponding author.

PII S0022-3115(97)00299-7

0.4 H/C at room temperature [11], i.e. similar to the saturation concentration at ion implantation. Codeposited hydrogen–carbon layers grow about linearly with the discharge time [12]. Thus the amount of hydrogen trapped by codeposition may largely exceed the amount trapped in the implantation zone and the amount trapped by migration into the bulk. Several kg of tritium may be trapped by codeposition in ITER [13]. The tritium inventory accumulated by codeposition depends both on the amount of eroded and redeposited carbon and the saturation concentration of hydrogen in the codeposited layers. It may be lowered if the erosion yield of carbon by hydrogen and/or the concentration of trapped hydrogen can be decreased.

A considerable effort has been undertaken to modify graphite by the addition of other elements such as B, Si, Ti or W to reduce the chemical erosion yield of graphite [17–26]. The influence of dopants on the hydrogen retention characteristics of carbon-based materials is, however, only little investigated. There is some hope that dopants may affect the saturation concentration or the migration behaviour. Haasz and Davis have examined the deuterium retention characteristics of specially manufactured graphites doped with 10–20 at.% B, Si, Ti or W by thermal desorption spectroscopy (TDS) [15]. They found, however, that dopants rather have a tendency even to increase the amount of trapped hydrogen. From the experiments it could not be deduced if the increase of hydrogen retention is due to a higher saturation concentration in the implantation zone or to an enhanced migration into the bulk.

In the present study we have investigated the hydrogen retention characteristics of commercially available graphites doped with low concentrations of boron, silicon and titanium as well as the hydrogen retention characteristics of the carbides B_4C, SiC and TiC. The total amount of retained hydrogen in the implantation zone and in the bulk was determined with thermal desorption spectroscopy (TDS), and the saturation concentration in the implantation zone was determined with ion beam analysis.

2. Experimental

2.1. Materials

The doped graphites investigated in the present study are listed in Table 1.

– The LS10 and LT10 materials contain 10 at.% Si and 10 at% Ti, respectively, and are isostatically pressed powder mixtures at 1600–2000°C with C-grain sizes of about 0.5 μm and the dopants in carbidic grains of SiC with a size of about 1.2–5 μm and TiC with about 1.4–3.3 μm grain size.

– The RG-Ti-91 material, provided by Efremov Institute, St. Petersburg, is a titanium doped recrystallized graphite produced from a mixture of graphite powder with Ti powder bound with coal tar pitch by pressing at 800 to 1000°C and subsequent high pressure annealing at 2500–3000°C. Further RG-Ti samples with boron additions of 0.1, 0.4, 0.8, 2 and 4 at.%, which have been manufactured by the same procedure, have been investigated.

– NS31 is a 3D silicon doped CFC material from the manufacturer SEP with a dopant concentration of 8–10 at%. NS31 has a high thermal conductivity and is currently considered as reference material for ITER.

– USB15 is a boronized graphite containing 15 wt% (16.4 at%) B. About 2–3 at.% B dissolves substitutionally in the graphite matrix, the rest precipitates in B_4C grains with a mean size of 5–10 nm [27].

Pyrolytic graphite from Union Carbide has been used as reference material. It is a polycrystalline material which has a density near the theoretical density of graphite and is nearly free of pores. However, there are enough internal grain boundaries to allow migration of implanted deuterium into the bulk [14].

The samples were polished with diamond paste, except NS31. For USB15, B_4C, SiC, TiC and pyrolytic graphite a smooth and shiny surface was obtained. The surface of the other materials still remained rough.

The dopant concentrations as provided by the manufac-

Table 1
Properties of the doped graphites used in the present study. The values for density and porosity were taken from the data sheets provided by the manufacturers

Material	Source	Dopant	Dopant concentration (at.%)	Density (g/cm^3)	Porosity (%)
USB15	NII Grafit Russia	B	16.4	2.0	10
LS10	CEREM France	Si	10	2.38	3.9
NS31	SEP France	Si	8–10	2.0	5
LT10	CEREM France	Ti	10	2.79	2.2
RG-Ti-91	Efremov Inst. Russia	Ti	1.7	2.23	
RG-Ti-B-91	Efremov Inst. Russia	Ti and B	1.7 (Ti), 0.1–4 (B)	2.23	
Pyrolytic graphite	Union Carbide	–	–	2.20	≈ 0

turers were checked with Rutherford backscattering analysis (RBS) at a scattering angle of 165° with 2 MeV incident He ions for Si and Ti and with nuclear reaction analysis (NRA) for B with a beam spot size of about 1 mm^2. All doped graphites except USB15 turned out to be inhomogeneous. The dopant concentration averaged over 1 mm^2 of the sample surface varied by about 30% at different spots.

2.2. Analysis

The deuterium implantations were performed at the Garching high current ion source [28] with 3 keV D_3^+ (yielding 1 keV per D) and 8 keV D^+ with a current density of about 110 $\mu A/cm^2$ and a beam spot size of about 0.45 cm^2. All implantations were performed at room temperature.

Thermal desorption spectroscopy (TDS) was performed in the same target chamber as the implantation by heating up to 1450 K with a linear heating ramp of about 6 ± 0.5 K/s. The temperature was measured with an infrared pyrometer. Mass 3 (HD), mass 4 (D_2) and mass 20 (CD_4) were monitored with a quadrupole mass spectrometer.

The implanted specimens were transported through air to the ion beam analysis chamber. The deuterium trapped in the surface layer of about 1 μm was determined by nuclear reaction analysis (NRA) using the $D(^3He,p)\alpha$ reaction at an incident energy of 790 keV and a beam spot size of about 1 mm^2. The protons from the nuclear reaction were detected with a large angle proton counter. The solid

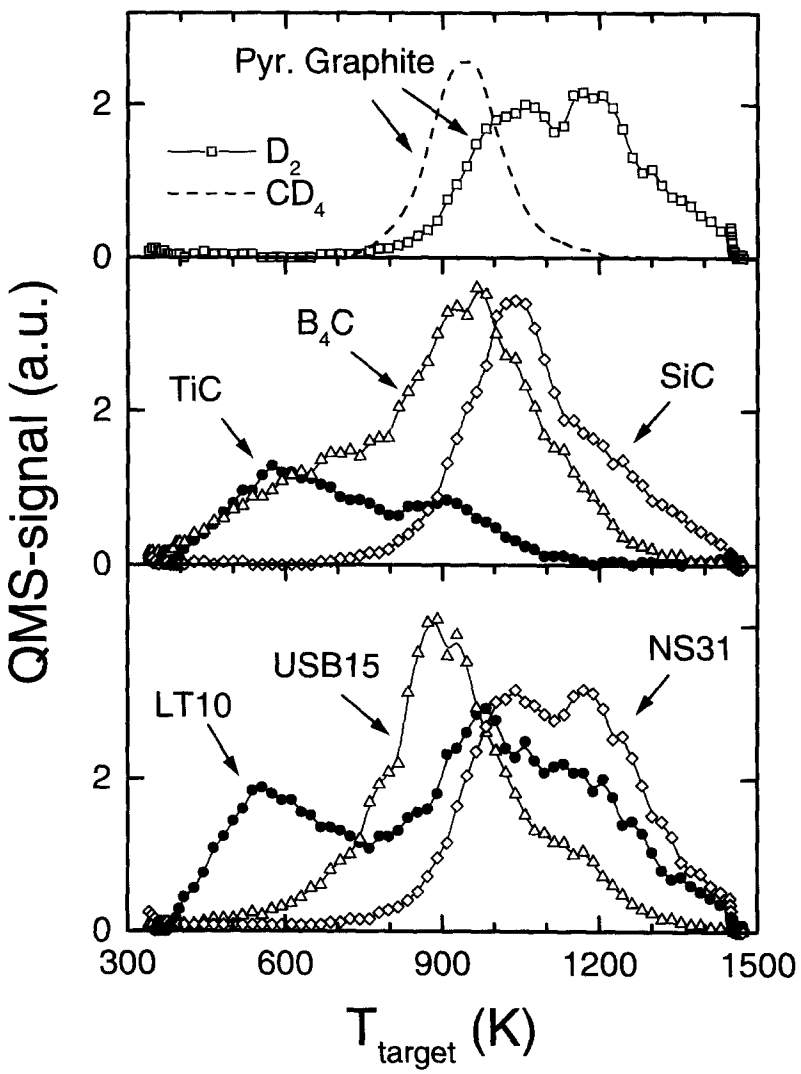

Fig. 1. TDS spectra of D_2 molecules released from pyrolytic graphite, carbides (B_4C, SiC, TiC), and doped graphites (USB15, NS31, LT10), implanted at room temperature with 1 keV per D and a fluence of 2.7×10^{18} D/cm^2. The TDS spectrum of CD_4 molecules for pyrolytic graphite is shown as a dotted line. All spectra were recorded with a linear heating ramp of about 6 K/s.

angle of the detector was calibrated with a calibrated target (D in Er). Depth profiles of D were obtained with the same nuclear reaction from the energy spectrum of the α-particles at a scattering angle of 102.5°. The energy spectra were converted to depth profiles with the program LORI [29].

All depth profiles obtained with ion beam analysis are given in atoms/cm^2. With the knowledge of the atomic density of the material (including porosity or swelling due to disorder or damage) the depth in at/cm^2 can be transformed to cm by dividing with the atomic density. For graphites 10^{15} at/cm^2 correspond roughly to 0.1 nm.

The integrated TDS signals were quantified by a comparison with the inventories measured by NRA for an implantation fluence of 2.7×10^{18} D/cm^2. The calibration factor for the D_2 signal was obtained by using the sum of the NRA inventories of the carbides, which produce no CD_4; then the calibration factor for the CD_4 signals was gained out of the average of the data of pyrolytic graphite and USB15.

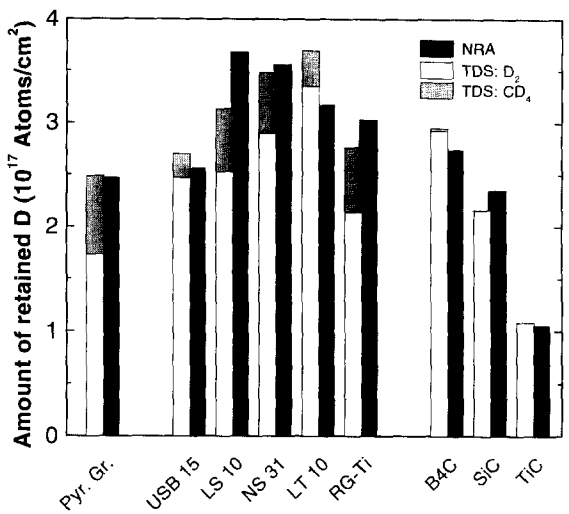

Fig. 3. Retained amount of D in the different materials for 1 keV D bombardment with a fluence of 2.7×10^{18} D atoms/cm^2. The retained amount was determined both with NRA and TDS.

3. Results and discussion

Typical thermal desorption spectra of D_2 molecules released from pyrolytic graphite, carbides (B_4C, SiC, TiC), and doped graphites (USB15, NS31, LT10) are presented in Fig. 1. All spectra were recorded with a linear heating ramp of about 6 K/s after D implantation at room temperature with 1 keV per D atom and a fluence of 2.7×10^{18} D/cm^2. The temperature of the desorption maximum decreases from pyrolytic graphite (1200 K, 1050 K), via SiC (1050 K) and B_4C (950 K) to TiC (600 K), indicating the different bond strengths of the trapped hydrogen [20,30,31]. The spectra of the doped graphites look like an overlay of the spectra of pyrolytic graphite and the corresponding carbide, perhaps with a small shift in the temperature of the maximum.

Additionally, the thermal desorption spectrum of CD_4 molecules for pyrolytic graphite is shown in Fig. 1 (dotted line). The spectrum consists of a single peak around 950 K. For all other materials the shape of the CD_4 peak looks similar but the intensity of the CD_4 signal is reduced due to the reduction of chemical erosion compared to pyrolytic graphite (see also Fig. 3). For the carbides no CD_4 release was found except for B_4C, where the CD_4 signal is just above the detection limit. For all CD_4 signals the shift in temperature of the desorption maximum is less than 50 K, except for USB15, where the temperature of the maximum is reduced by about 100 K.

The retention of deuterium for 1 keV bombardment at room temperature as a function of the incident fluence is shown in Fig. 2 for pyrolytic graphite, RG-Ti with 4% B, LT10 and NS31. The total amount of retained deuterium was determined with TDS and quantified with the aid of the NRA data, as described above. For fluences below

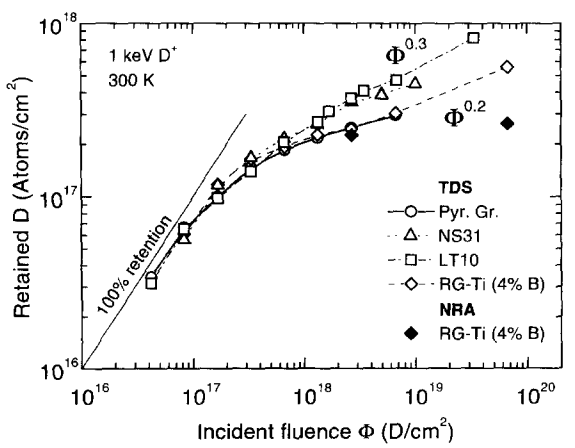

Fig. 2. Fluence dependence of the retained amount of deuterium in pyrolytic graphite, LT10, RG-Ti-91 with 4 at.% B and NS31 for bombardment with 3 keV D_3^+ at room temperature.

Table 2
Mean ranges of 1 keV and 8 keV D in B_4C, graphite, SiC, and TiC calculated with the program TRIM.SP. The mean ranges are given in atoms/cm^2, with 10^{15} atoms/cm^2 corresponding roughly to 0.1 nm, depending on the atomic density of the material

Material	Mean range (atoms/cm^2)	
	1 keV	8 keV
B_4C	2.5×10^{17}	1.8×10^{18}
Graphite	2.3×10^{17}	1.6×10^{18}
SiC	1.8×10^{17}	1.2×10^{18}
TiC	1.6×10^{17}	9.7×10^{17}

$\approx 10^{17}$ D/cm^2, all of the non-reflected deuterium is retained in the specimens. For higher fluences local saturation within the implanted layer occurs and deuterium is reemitted, resulting in a levelling off of the retained amount of deuterium. A stationary inventory however is not reached, and the retained amount still increases until the highest fluences used in the experiments. This was observed earlier by Haasz and Davis for porous and doped graphites [14,15] and it was interpreted as migration of deuterium atoms along grain boundaries or pores beyond the implantation zone into the bulk material [10]. Only for pseudo-monocrystalline graphite, such as highly oriented pyrolytic graphite (HOPG), a stationary inventory and no further increase with incident fluence was observed [14].

Fig. 2 shows the fluence dependence of the retained deuterium in the investigated materials as obtained with TDS. Two data points are included where the deuterium inventory in RG-Ti-91 with 4% B was determined with NRA, which has an information depth of about 1.3×10^{19} atoms/cm^2 (1.3 μm). From a fluence of 2.7×10^{18} D/cm^2

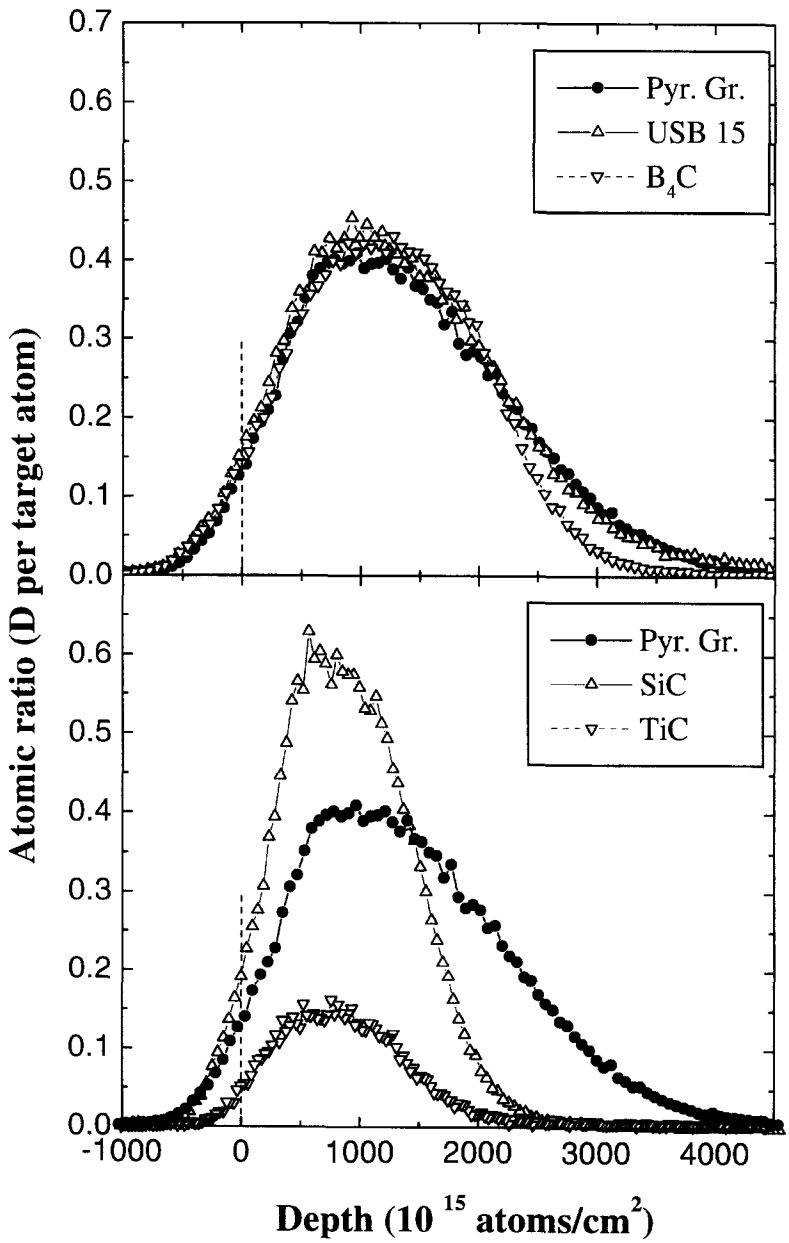

Fig. 4. Depth profiles of 8 keV D implanted in pyrolytic graphite, USB15, B_4C, SiC and TiC as obtained with NRA. The depth scale is given in 10^{15} atoms/cm^2, with 10^{15} atoms/cm^2 corresponding roughly to 0.1 nm, depending on the atomic density of the material.

to a fluence of 6.7×10^{19} D/cm^2 the amount of retained deuterium determined with NRA increases only slightly, whereas the amount determined with TDS increases by more than a factor 2. Because the NRA method probes only the surface layer whereas TDS determines also the inventory trapped in larger depths, this indicates clearly that deuterium migrates into depths larger than probed with NRA (> 1.3 μm).

The amount of deuterium trapped at room temperature in the RG-Ti materials with different boron additions between 0 and 4 at.% was found to be nearly identical in TDS and NRA measurements within the experimental errors; thus only the results for RG-Ti with 4% B are shown in Fig. 2.

For the high fluences the increase of the deuterium inventory with incident fluence is larger for NS31 and LT10 than for pyrolytic graphite and the RG-Ti materials. The increase is about linear in the double logarithmic plot. The retained amount of deuterium increases with the incident fluence with a power of 0.2 for pyrolytic graphite and the RG-Ti materials and a power of 0.3 for NS31 and LT10.

The amount of trapped deuterium atoms for 1 keV bombardment with a fluence of 2.7×10^{18} D atoms/cm^2 is compared in Fig. 3 for the different materials. At this fluence for all materials the results obtained with TDS and NRA are nearly identical (see also Fig. 2), indicating that only a small amount of D has migrated beyond the information depth of the NRA method.

In pyrolytic graphite a total amount of 2.5×10^{17} D atoms/cm^2 is trapped. All B, Si and Ti doped graphites exhibit a comparable or even higher deuterium inventory. Especially the inventory in the doped graphites LS10, NS31 and LT10 is a factor of about 1.5 higher than in pyrolytic graphite. The deuterium inventory in USB15 and in the RG-Ti-91 materials is only slightly higher than in pyrolytic graphite. The addition of boron in the range of 0.1–4 at.% to RG-Ti does not change the deuterium trapping at room temperature significantly. Our measured fraction of D atoms released as CD_4 and the total amount of D are in the same range as data obtained from literature [8,20,21]. The contradiction to [20] in the total amount of D retained in TiC could be explained by the 25% graphite in the TiC used there.

Most of the dopants are present in the form of carbides. The retention of deuterium in B_4C, SiC and TiC is shown in Fig. 3 as well. B_4C and SiC trap about the same total amount of D as pyrolytic graphite (for comparison [3,4,30–33]). Only TiC shows a deuterium inventory which is a factor of about 2.5 lower than the inventory in pyrolytic graphite [3,4]. In the titanium doped material LT10 most of the titanium is present in the form of TiC. However, the deuterium inventory in LT10 is higher than in pyrolytic graphite and not lower, which would be expected from the lower inventory in TiC. The same tendency is visible for the other doped graphites. This is another clear indication that diffusion into the bulk is responsible for the higher deuterium inventories.

The total amount of retained deuterium for low fluence implantation depends both on the saturation concentration in the implantation zone and the range of the incident particles. In order to obtain information about the saturation concentration of deuterium in the implantation zone deuterium was implanted with 8 keV and analyzed with NRA. For lower implantation energies the mean range of the implanted D is lower than the depth resolution of the NRA method. The mean ranges of 1 keV and 8 keV deuterium in B_4C, graphite, SiC and TiC were calculated with the program TRIM.SP [34–36] and are shown in Table 2. Due to the higher electronic stopping power of elements with higher Z the mean range decreases from B_4C to SiC and TiC.

The depth profiles of 8 keV D implanted in pyrolytic graphite, USB15, B_4C, SiC and TiC are shown in Fig. 4. Due to the surface roughness of the other materials no reliable depth profiles could be obtained for the RG-Ti materials, LT10, LS10 and NS31. The depth scale in Fig. 4 is given in 10^{15} atoms/cm^2, with 10^{15} atoms/cm$^2 \approx 0.1$ nm. The depth resolution of the method is about 1000×10^{15} atoms/cm^2.

The measured saturation concentration of D in pyrolytic graphite is 0.4 D/C, which is in good agreement with previous measurements [2–10]. Also the experimentally determined mean range is in good agreement with the calculated results from Table 2. The addition of boron does not alter the saturation concentration significantly. In USB15 and B_4C nearly the same saturation concentration as in graphite is observed.

The measured saturation concentration of D in SiC is about 0.6 D atoms per target atom and therefore a factor of 1.5 higher than in graphite. Due to the smaller implantation range (Fig. 4 and Table 2) the total amount of deuterium trapped in SiC is about the same as in graphite for monoenergetic implantation. In TiC the measured saturation concentration is 0.15 D atoms per target atom and therefore a factor of 2.7 lower than in graphite. TiC has also the smallest implantation range due to the highest stopping power. At the fluence used in this experiment there is no migration of deuterium into the bulk material observable.

4. Conclusions

The trapping of 1 keV and 8 keV deuterium implanted into B, Si and Ti doped graphites and the carbides B_4C, SiC and TiC up to fluences of 6.7×10^{19} D/cm^2 has been studied at room temperature with TDS and NRA. Pyrolytic graphite has been used as reference material. All doped graphites investigated in this study tend to retain a larger

amount of deuterium than pyrolytic graphite. A stationary deuterium inventory is not reached, but the total inventory still increases up to the highest implantation fluences. This increase at high fluences is attributed to the migration of implanted deuterium into the bulk along grain boundaries or pores, in agreement with previous measurements [14,15]. The migration of deuterium into the bulk material depends on the microstructure (grain boundaries, porosity) of the graphite material. All doped graphites tend to have a higher porosity than pyrolytic graphite.

The saturation concentration of deuterium in graphite is 0.4 D/C at room temperature. The carbide B_4C shows about the same saturation concentration for 8 keV implantation. In SiC the saturation concentration is 0.6 D atoms per target atom and therefore a factor of 1.5 higher than in graphite. Only TiC shows a much lower deuterium inventory than graphite. The saturation concentration of D in TiC is 0.15 D atoms per target atom. In the literature a broad variety of different manufactured carbides and graphites was investigated with the same tendency for B_4C, SiC, and TiC in comparison to graphite [2–6,32,33,37].

For the tritium inventory in next step fusion devices the amount of hydrogen trapped by codeposition is of crucial importance. In a previous paper [11,38] we have developed a simple model which allows the prediction of the amount of hydrogen codeposited with a given material. This model is valid if the incident hydrogen has high energies. We have called this model coimplantation. During the layer growth the growing layer is bombarded with hydrogen until saturation. In the frame of this model the concentration of codeposited hydrogen is equal to the saturation concentration obtained in ion beam implantation experiments. Due to the higher saturation concentration of hydrogen in SiC, silicon doped graphites and silicon carbide should trap a larger amount of hydrogen by codeposition than pure carbon. This is also observed for plasma deposited a-Si/C:H films produced in glow discharges, where the highest hydrogen inventories are measured for films with Si:C $\approx$ 1 [39]. However, due to the lower erosion yield of silicon doped graphites by hydrogen the amount of material available for codeposition is reduced. From the viewpoint of the total amount of trapped hydrogen by codeposition it is hard to decide whether silicon doped graphites or SiC are better or worse than pure graphite. Definitely, this depends on the plasma parameter. The only material investigated in this study which seems to be advantageous compared to pure carbon is TiC. TiC has a lower erosion yield compared to carbon, thus reducing the amount of material available for codeposition, and a saturation concentration of hydrogen which is a factor of 2.7 lower than in carbon. Additionally, the trapped deuterium can be removed at lower temperatures. However, if under the conditions of simultaneous bombardment with hydrogen, carbon and titanium, TiC with its good properties will be formed, that needs further experimental justification.

References

[1] G. Federici, R. Anderl, J.N. Brooks, R. Causey, J.P. Coad, D. Cowgill, R. Doerner, A.A. Haasz, G. Longhurst, S. Luckhardt, D. Mueller, A. Peacock, M. Pick, C. Skinner, W. Wampler, K. Wilson, C. Wong, C. Wu, D. Youchison, Tritium inventory in the ITER PFCs: Predictions, uncertainties, R&D status and priority needs, presented at the ISFNT-4, Tokyo, Japan, April 6–11, 1997, Fus. Eng. Des., to be published.

[2] G. Staudenmaier, J. Roth, R. Behrisch, J. Bohdansky, W. Eckstein, P. Staib, S. Matteson, S.K. Erents, J. Nucl. Mater. 84 (1979) 149.

[3] B.L. Doyle, W.R. Wampler, D.K. Brice, S.T. Picraux, J. Nucl. Mater. 93&94 (1980) 551.

[4] B.L. Doyle, D.K. Brice, W.R. Wampler, IEEE Trans. Nucl. Sci. 28 (1981) 1300.

[5] W.R. Wampler, D.K. Brice, C.W. Magee, J. Nucl. Mater. 102 (1981) 304.

[6] M. Braun, B. Emmoth, J. Nucl. Mater. 128&129 (1984) 657.

[7] W. Möller, B.M.U. Scherzer, J. Appl. Phys. 64 (1988) 4860.

[8] W. Möller, J. Nucl. Mater. 162–164 (1989) 138.

[9] K.L. Wilson, R. Bastasz, R.A. Causey, D.K. Brice, B.L. Doyle, W.R. Wampler, W. Möller, B.M.U. Scherzer, T. Tanabe, in: Atomic and Plasma–Material Interaction Data for Fusion, Suppl. J. Nucl. Fusion, IAEA, Vienna, 1991, p. 31.

[10] A.A. Haasz, P. Franzen, J.W. Davis, S. Chiu, C.S. Pitcher, J. Appl. Phys. 77 (1995) 66.

[11] M. Mayer, R. Behrisch, H. Plank, J. Roth, G. Dollinger, C.M. Frey, J. Nucl. Mater. 230 (1996) 67.

[12] G. Federici, R. Causey, P.L. Andrew, C.H. Wu, Fus. Eng. Des. 28 (1995) 136.

[13] G. Federici, D. Holland, G. Janeschitz, C.H. Wu, J. Nucl. Mater. 241–243 (1997) 260.

[14] A.A. Haasz, J.W. Davis, J. Nucl. Mater. 209 (1994) 155.

[15] A.A. Haasz, J.W. Davis, J. Nucl. Mater. 232 (1996) 219.

[16] P. Franzen, R. Behrisch, C. García-Rosales, The ASDEX Upgrade Team, D. Schleussner, D. Rösler, J. Becker, W. Knapp, Ch. Edelmann, Nucl. Fus. 37 (1997) in press.

[17] J. Roth, E. Vietzke, A.A. Haasz, in: Atomic and Plasma–Material Interaction Data for Fusion, vol. 1, Nucl. Fus. Special Issue, IAEA, Vienna, 1991, p. 63.

[18] C. García-Rosales, E. Gauthier, J. Roth, R. Schwörer, W. Eckstein, J. Nucl. Mater. 189 (1992) 1.

[19] C. García-Rosales, J. Roth, J. Nucl. Mater. 196–198 (1992) 573.

[20] C. García-Rosales, J. Roth, R. Behrisch, J. Nucl. Mater. 212–215 (1994) 1211.

[21] V.Kh. Alimov, R. Schwörer, B.M.U. Scherzer, J. Roth, J. Nucl. Mater. 187 (1992) 191.

[22] R. Schwörer, J. Roth, J. Appl. Phys. 77 (1995) 3812.

[23] H. Plank, R. Schwörer, J. Roth, Nucl. Instrum. Meth. B 111 (1996) 63.

[24] H. Plank, R. Schwörer, J. Roth, Surf. Coat. Technol. 83 (1996) 93.

[25] J. Roth, H. Plank, R. Schwörer, Phys. Scripta T 64 (1996) 67.

[26] R. Schwörer, H. Plank, J. Roth, J. Nucl. Mater. 230 (1996) 208.

[27] V.N. Chernikov, V.Kh. Alimov, A.E. Gorodetsky, V.M.

Shaparov, A.P. Zakharov, E.I. Kurolenkin, J. Nucl. Mater. 191–194 (1992) 320.
[28] W. Eckstein, C. García-Rosales, J. Roth, W. Ottenberger, Sputtering Data, Tech. Rep. IPP 9/82, Max-Planck-Institut für Plasmaphysik, Garching, 1993.
[29] B.M.U. Scherzer, H.L. Bay, R. Behrisch, P. Børgesen, J. Roth, Nucl. Instrum. Meth. 157 (1978) 75.
[30] Y. Yamauchi, Y. Hirohata, T. Hino, T. Yamashima, T. Ando, M. Akiba, J. Nucl. Mater. 220–222 (1995) 851.
[31] Y. Yamauchi, T. Hino, Y. Hirohata, T. Yamashima, Vacuum 47 (1996) 973.
[32] S. Nagata, S. Yamaguchi, Y. Fujino, M. Hirabayashi, K. Kamada, J. Nucl. Mater. 128&129 (1984) 760.
[33] R. Siegele, S.P. Withrow, J. Roth, B.M.U. Scherzer, J. Nucl. Mater. 176&177 (1990) 1010.
[34] J.P. Biersack, W. Eckstein, Appl. Phys. A 34 (1984) 73.
[35] W. Eckstein, Computer Simulation of Ion–solid Interactions, vol. 10, Mater. Sci., Springer, Berlin, 1991.
[36] M. Mayer, W. Eckstein, Nucl. Instrum. Meth. B 94 (1994) 22.
[37] R. Jimbou, M. Saidoh, N. Ogiwara, T. Ando, M. Morita, Y. Muto, J. Nucl. Mater. 196–198 (1992) 958.
[38] M. Mayer, J. Nucl. Mater. 240 (1997) 164.
[39] F. Demichelis, F. Giorgis, C.F. Pirri, E. Tresso, Philos. Mag. A 72 (1995) 913.